

Absolute Broadband Polarization Behaviour of PSR B0329+54: A Glimpse of the Core Emission Process

Dipanjan Mitra¹, Joanna M. Rankin² & Yashwant Gupta¹

¹*National Centre for Radio Astrophysics, Ganeshkhind, Pune 411 007 India : dmitra@ncra.tifr.res.in; ygupta@ncra.tifr.res.in*

²*Physics Department, University of Vermont, Burlington, VT 05405 USA : Joanna.Rankin@uvm.edu*

Released 2004 Xxxxx XX

ABSTRACT

In this paper we report multifrequency single pulse polarization observations of the PSR B0329+54 normal mode using the Giant Meterwave Radio Telescope at 325 and 610 MHz and the Effelsberg Observatory at 2695 MHz. Our observations show that towards the central part of the polarization position-angle traverse there is an unusual “arc”-like structure, which is comprised of a broadband “kink” and a frequency-dependent “spot.” The features are intimately connected with the intensity dependence of the core component as well as being closely associated with the nearly complete negative circular polarization on its trailing edge. We find that the “kink” emission is associated with the extraordinary (X) propagation mode, and hence propagation effects do not appear capable of producing the core component’s broadband, intensity-dependent emission. Rather, the overall evidence points to a largely geometric interpretation in which the “kink” provides a rare glimpse of the accelerating cascade or height-dependent amplifier responsible for the core radiation.

Key words: miscellaneous – methods:MHD — plasmas — data analysis – s: general, individual (B0329+54) — radiation mechanism: nonthermal – polarization.

I. INTRODUCTION

Radio pulsars are well known to emit highly polarized radiation. Radhakrishnan & Cooke (1969; hereafter R&C) observed the Vela pulsar and demonstrated that the linear polarization position angle (PA) across its average-pulse profile exhibits a characteristic ‘S-shaped’ traverse. This PA-longitude dependence was interpreted as reflecting the varying projected magnetic field direction within an overall dipolar configuration (R&C; Komesaroff 1970). According to this rotating-vector model (RVM), wherein the received emission is associated with those field lines (momentarily) having tangents along our sight-line direction, the linear polarisation will be oriented within this tangent plane, varying with the neutron star’s rotation. The PA χ as a function of pulse longitude φ can then be represented as

$$\chi = \tan^{-1} \left(\frac{\sin \alpha \sin \varphi}{\sin \xi \cos \alpha - \sin \alpha \cos \xi \cos \varphi} \right). \quad (1)$$

(Manchester & Taylor 1977) where α is the magnetic latitude and β the sightline impact angle such that $\xi = \alpha + \beta$.

The RVM strongly suggests that pulsar radiation is highly beamed and results from relativistic charged particles moving along the open dipolar magnetic field lines producing curvature radiation. This simple RVM model, however has had difficulty in explaining the wide diversity

of average PA traverses (*e.g.*, Gould & Lyne 1998; Hankins & Rankin 2006) observed in pulsar average profiles. Most pulsars, for instance, exhibit orthogonal polarization modes (OPMs) wherein the PAs are found to have two preferred values at a given pulse longitude differing by about 90° (Manchester *et al* 1975; Backer & Rankin 1980). The relative strengths of the modes vary with longitude causing the average PA traverse to exhibit “90° jumps”. Even when these modal effects are carefully considered, many pulsars show average PA behaviours that are inconsistent with the RVM (Everett & Weisberg 2001; Ramachandran *et al* 2004). Individual pulse studies, however, more clearly delineate OPM effects, and the behaviour of each mode is more usually found to be consistent with the RVM.

Pulsar B0329+54 provides a fascinating context for investigating detailed polarization behaviour. Discovered in 1968 and reported in the third and final Cambridge “batch” (Cole & Pilkington 1968), it is one of the brightest pulsars in the northern sky and has thus been studied both early and very extensively, often with the Effelsberg 100-m telescope at 1700 MHz. One such classic study by Bartel *et al* (1982; hereafter BMSH) carefully delineated the properties of its profile and polarisation modes. A more recent observation by Gil & Lyne (1995; hereafter GL95) using the Lovell instrument at 408 MHz exhibited the remarkable complexity

of the object's PA behaviour and simulated Mitra (1999) to investigate the physical origins of its non-RVM effects. Referring to GL95's fig. 1, we see that the pulsar's average PA is distorted by the presence of the two OPMs over much of its duration. The individual pulse PAs are well enough confined to the two modal "tracks", though, that consistent, reliable fits to eq.(1) could be made to them. These authors do also note, however, that the emission shows significant departures from the RVM within a region near the center of the profile associated with its core component—a fact noted earlier as well using modal profiles by Gil *et al* (1992).

Peculiar PA behaviour has been noted in a number of other pulsars within the longitude range of the central core component (*e.g.*, Rankin 1983a, 1990; hereafter R83a, R90). In the core-cone emission model, the central core and outlying conal components are thought to be produced by a central "pencil" beam within a hollow radiation cone. In such configurations (of which B0329+54 is an excellent example), the RVM behaviour is most clearly associated with the conal components and is thus often interrupted or distorted in the core region. This apparent non-RVM emission has even prompted speculation that the core might be produced by a different emission mechanism than that of the cone (*e.g.*, Radhakrishnan & Rankin 1990), but this conjecture has attracted no satisfactory theoretical grounding.

More recently, Malov & Suleymanova (1998; hereafter MS98) as well as Gangadhara & Gupta (2001; hereafter G&G) have attempted to interpret B0329+54's emission configuration on the basis of aberration and retardation (hereafter A/R), taking its bright central feature as the core component and thus as the profile center and then computing emission heights for its several cones. The latter authors also find evidence for several new emission components, and we will use their designations below (see their fig. 3). And in two other papers Suleymanova & Pugachev (1998, 2002; SP98/02) first analyse the linear polarisation distributions at 103 and 60 MHz and then study transitions between the pulsar's "abnormal" and "normal" profile modes at 111 MHz. Karastergiou *et al* (2001) study how power and polarisation are correlated in simultaneous observations at 1.41 and 2.69 GHz.

Edwards & Stappers (2004; hereafter ES04) have published a major study of the pulsar's OPM properties using new high quality 328-MHz polarimetric observations from the Westerbork Synthesis Radio Telescope (WSRT). Their novel analysis delineates the character of the star's OPM behaviour in detail, and on this basis they speculate about its physical origins. Their study underscores the importance of understanding this star's non-RVM, core-component properties in the full context of both current analyses and the rich published literature. We will make considerable use of ES's results in our work below.

Currently, a number of divergent ideas have arisen in the course of efforts to understand OPM anomalies: GL95 explained their results as an effect of finite beamwidth wherein radiation from nearby field lines was superposed within the sightline. Further, they argued that this effect is more severe near the polar cap from where the field lines diverge. (In general, however, radiation from nearby field lines should superpose symmetrically and should not affect the overall PA traverse; a very special circumstance is thus needed to produce the observed non-RVM behaviour.) Mitra *et al* (2000)

Table 1. Single-Pulse Polarimetry Observations

Telescope		BW	Resolution	Pulses	
Frequency	Date	(MHz)	(MHz)	(#)	
		channels	(°)	Mode	
GMRT	2004	16	0.512	2970	
325	27 Aug	256	0.26		normal
GMRT	2005	0.16	0.512	1650	
610	1 Jun	128	0.26		normal
Effelsberg	1997	80	0.697	2267	
2650	19 Oct	128	0.35		normal

thus attributed this effect to multipolar magnetic field contributions in the core-emission region. More recently Mitra & Sieradakis (2004) have speculated that A/R resulting from height-dependent emission can cause distorted PA traverses, and ES04 appeal to magnetospheric refraction to the same end. Srostlik & Rankin (2005) have shown that OPM's associated with the core emission in B1237+25 can distort the average PA traverse. Ramachandran *et al* (2004) attributed PA anomalies in B2016+28 to return currents in the pulsar magnetosphere. Given the multitude of possible explanations available, it is clear that primary new observational and analytical work on the OPM phenomenon is needed, especially in the core-emission context. Some important constraints, for instance, can be obtained by studying the frequency dependence of the OPM phenomena responsible for the non-RVM PA behaviours.

Furthermore, B0329+54's bright central component exhibits a clear intensity dependence: At low intensities its peak lies most of a degree later than at high intensities as shown by McKinnon & Hankins' (1993; hereafter MH93) fig. 1. They also find that the overall profile width decreases with increasing intensity. Such behaviour is unusual, although the Vela pulsar B0833-45 is also known to exhibit a similar effect (Krishnamohan & Downs 1983; hereafter KD83). Such an overall shift in the central component position is also seen between the pulsar's two profile modes, such that the abnormal lags the normal by some 0.5°. (see BMSH: fig. 3 or SP02: fig. 1). We will see below that B0329+54's non-RVM effects are closely associated with the intensity-dependent position of its central component—and thus perhaps this aspect of its profile mode shifts—so any proposed physical explanation must consider both phenomena.

In this paper we revisit the issues encountered in understanding the PA distributions of pulsar B0329+54 using high quality polarimetry spanning a some three octaves. In §II we give details of the observations and their preparation for analysis. §III discusses the multifrequency PA distributions, and §IV considers means to segregate the RVM and non-RVM behaviours. In §V we discuss the several distinct contributions to core power, §VI then reviews evidence pertaining to PSR B0329+54's basic emission geometry as well as efforts to confirm and extend it. and §VII provides a discussion and review of the results.

II. OBSERVATIONS

Pulse-sequence (hereafter PS) polarisation observations of pulsar B0329+54's 'normal' mode at 325, 610 and 2650

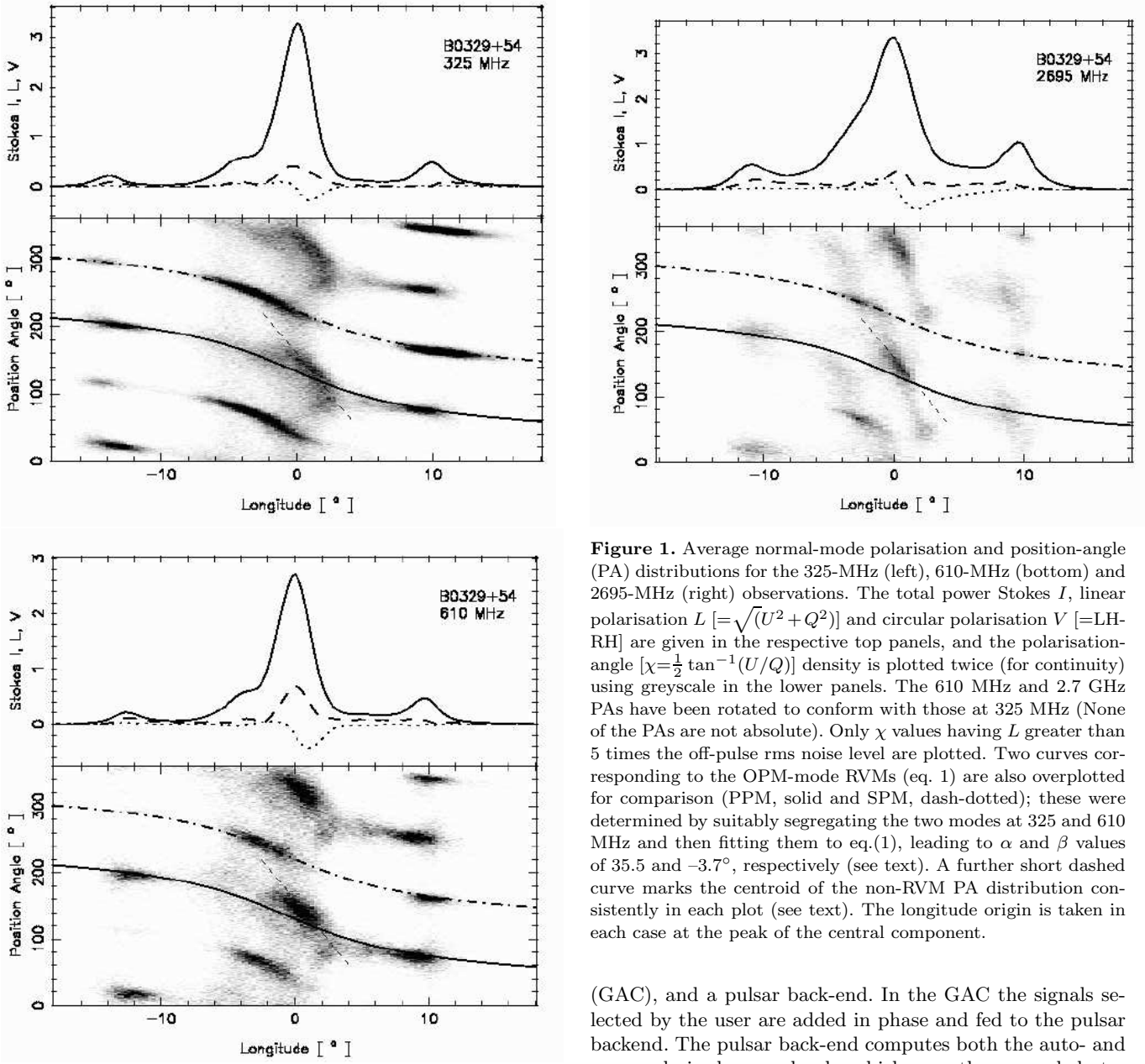


Figure 1. Average normal-mode polarisation and position-angle (PA) distributions for the 325-MHz (left), 610-MHz (bottom) and 2695-MHz (right) observations. The total power Stokes I , linear polarisation L [$-\sqrt{U^2 + Q^2}$] and circular polarisation V [$-LH - RH$] are given in the respective top panels, and the polarisation-angle [$\chi = \frac{1}{2} \tan^{-1}(U/Q)$] density is plotted twice (for continuity) using greyscale in the lower panels. The 610 MHz and 2.7 GHz PAs have been rotated to conform with those at 325 MHz (None of the PAs are not absolute). Only χ values having L greater than 5 times the off-pulse rms noise level are plotted. Two curves corresponding to the OPM-mode RVMs (eq. 1) are also overplotted for comparison (PPM, solid and SPM, dash-dotted); these were determined by suitably segregating the two modes at 325 and 610 MHz and then fitting them to eq.(1), leading to α and β values of 35.5 and -3.7° , respectively (see text). A further short dashed curve marks the centroid of the non-RVM PA distribution consistently in each plot (see text). The longitude origin is taken in each case at the peak of the central component.

MHz are described in Table 1 and presented below. The 325- and 610-MHz PSs were acquired using the Giant Metrewave Radio Telescope (GMRT) near Pune, India and the 2695-MHz observations were made with the 100-m Effelsberg telescope, near Bonn, Germany. The GMRT is a multi-element aperture-synthesis telescope (Swarup *et al* 1991) consisting of 30 antennas distributed over a 25-km diameter area which can be configured as a single dish both in coherent and incoherent array modes of operation. The polarimetric observations discussed here used the coherent (or more commonly called ‘phased array’) mode (Gupta *et al* 2000; Sirothia 2000) in the upper of the two 16-MHz ‘sidebands’. At either frequency right- and left-hand circularly polarized complex voltages arrive at the sampler from each antenna. The voltage signals are subsequently sampled at the Nyquist rate and processed through a digital receiver system consisting of a correlator, the GMRT array combiner

(GAC), and a pulsar back-end. In the GAC the signals selected by the user are added in phase and fed to the pulsar backend. The pulsar back-end computes both the auto- and cross-polarized power levels, which were then recorded at a sampling interval of 0.512 msec. A suitable calibration procedure as described in Mitra *et al* (2005) is applied to the recorded data to get the calibrated Stokes parameters I , Q , U and V . The PS at 2695 MHz is an archival Effelsberg observation. The polarimetry there was carried out with a multiplying polarimeter and calibrated using the procedure described by von Hoensbroech & Xilouris (1997) and von Hoensbroech (1999). The calibrated Stokes PSs at all the frequencies were finally converted into European Pulsar Network (EPN, Lorimer *et al* 1998) format for offline analysis.

III. FREQUENCY DEPENDENCE OF POLARIZATION PROPERTIES

The three panels of Figure 1 give grey-scale representations of B0329+54’s (normal mode) PA occurrence frequency as a function of longitude for 325, 610 and 2695 MHz (upper

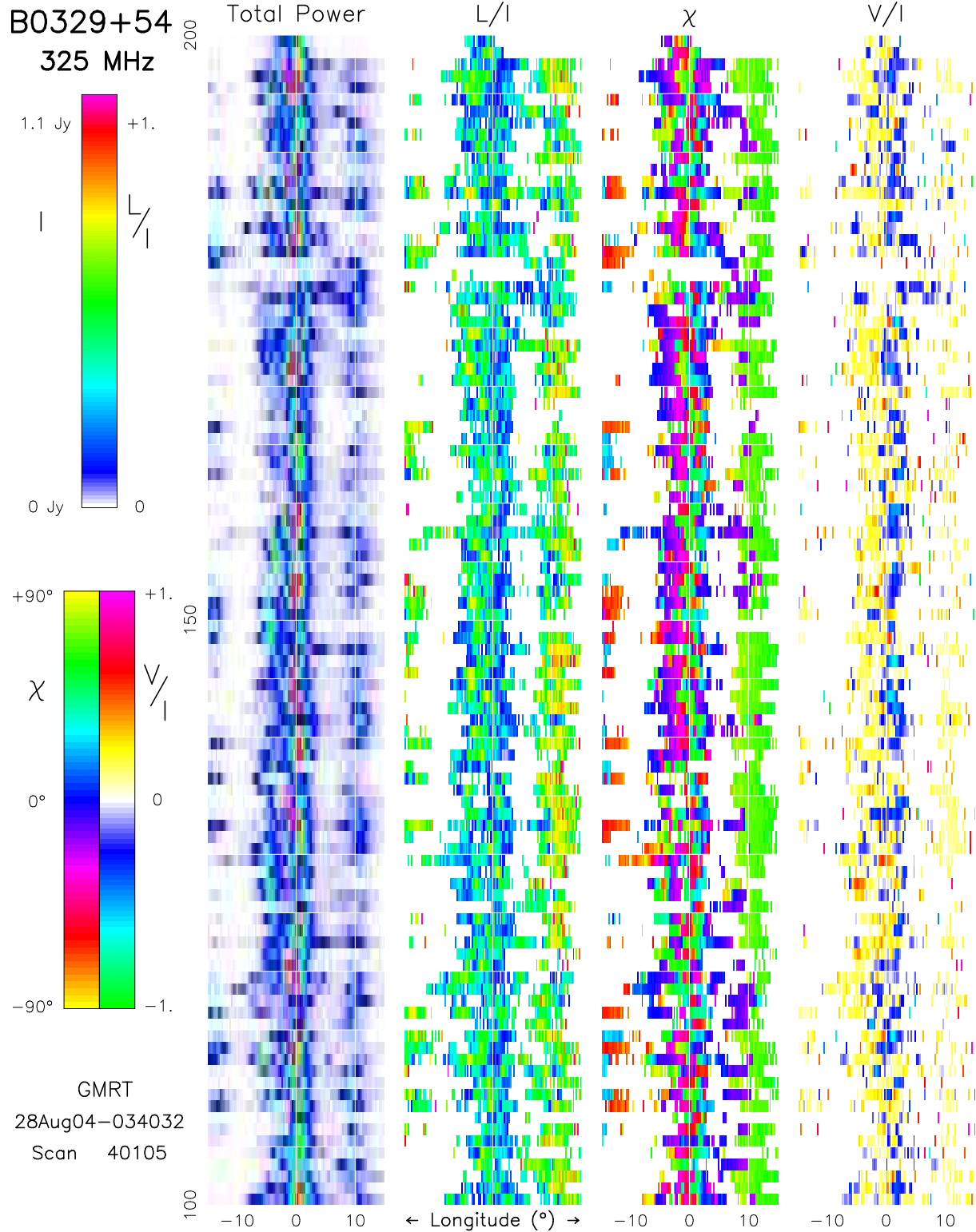


Figure 2. Pulse-sequence polarization display showing a 100-pulse section of the 325-MHz observations in Fig. 1 (top left). The (un-calibrated) total power I , fractional linear L/I , PA χ , and fractional circular polarization V/I are colour-coded in each of four columns according to their respective scales at the left of the diagram. Note that the intensity of the central core component varies strongly, from being undetectable during “core nulls” (e.g., pulses 180–181) to nearly saturating the intensity scale (pulses 196–197). Note also that while much of the “typical” core emission just follows the central longitude, the strongest such pulses tend to fall nearly on it or even precede it—that is, about 1° earlier. Both the background noise level and interference level of this observation is exceptionally low with the latter effectively disappearing into the lowest intensity white portion of the I color scale.

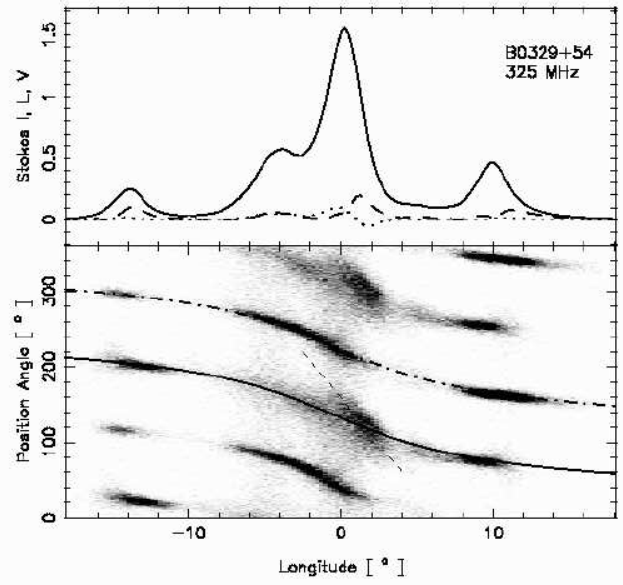
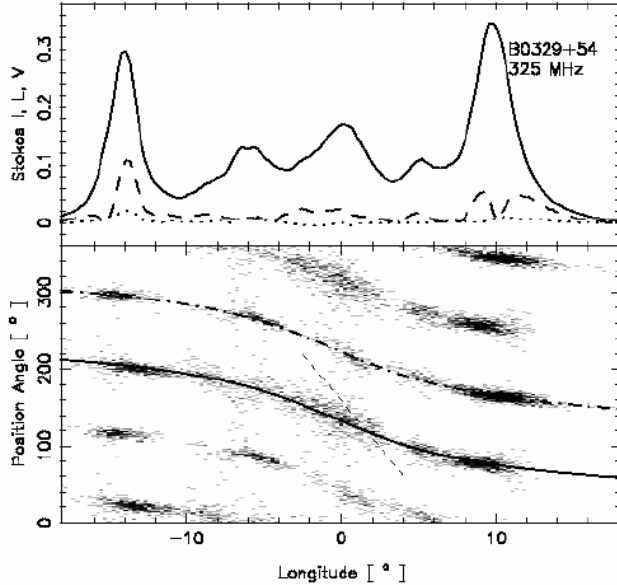
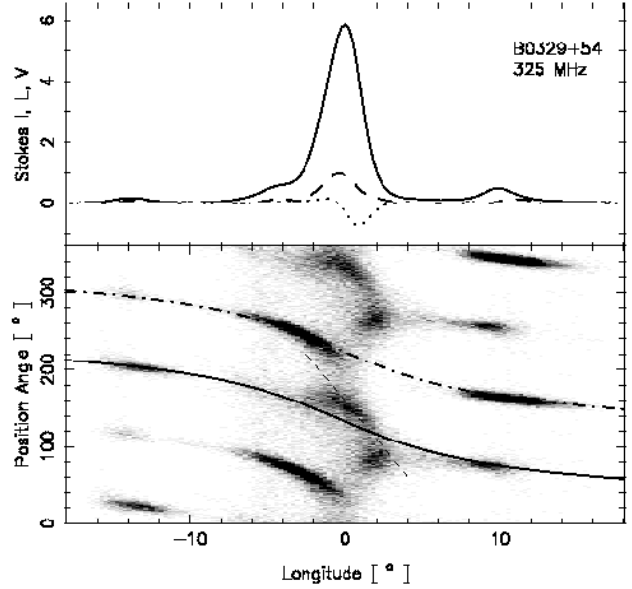


Figure 3. Average polarisation and position-angle (PA) distributions after Fig. 1 for three intensity sections of the 325-MHz observation corresponding to signal-to-noise ratio (hereafter S/N) levels of unity (left), 2–7 (right top), and 8–12 (right bottom). Distinguished on a pulse-by-pulse basis primarily according to the intensity of the bright central feature, the average profile changes from having five clear components at the lowest levels to exhibiting little more than the central feature at the highest ones. Note that the PA distributions at the lowest intensities accurately follow RVM ‘‘tracks’’; whereas, those with higher levels of central component power exhibit increasingly pronounced non-RVM PA effects. In particular, note that at intermediate intensities (right top) the linear PPM ‘‘kink’’ lies under the trailing part of the central component just above the PPM RVM track, but at the highest levels the ‘‘kink’’ departs maximally from the track and is centered under the perceptibly shifted central component. The trailing ‘‘spot’’ below the PPM track is seen only at the highest intensity levels. The three partial PA distributions represent 305, 1778 and 1191 pulses, respectively.

left, bottom and right), respectively. The 180° PA range is given twice for clarity, and an RVM model (discussed below) is overplotted along both the ‘‘primary’’ (solid) and ‘‘secondary’’ (dash-dotted curve) polarisation modes (hereafter, PPM and SPM) tracks. These displays are similar to GL95’s fig. 1 at 408 MHz but are more sensitive, better resolved and plotted with more grey levels. Comparing Fig. 1 (left)—our closest frequency at 325 MHz—with GL95, we see that the PA traverses are very similar. ‘‘Tracks’’ corresponding to the OPMs can readily be identified, and the less complex SPM track appears to exhibit a near perfect RVM behaviour.

It is the PPM track, however, which draws the eye: It too exhibits a clear RVM behaviour, but additionally we see a much steeper ‘‘kinky’’ area under the bright central feature. This region of conspicuously non-RVM dependence within the PA distribution, which has been noted in earlier studies as mentioned above, is one of the clearest such examples in any pulsar, and we thus take it as the main subject of this investigation.

This steeper, linear feature near the center of the profile is also visible in GL95’s fig. 1, but much less clearly—



though these authors do note a ‘‘significant amount of non-orthogonal radiation around the centre of the pulse’’. The greater sensitivity of the GMRT as well as a finer resolution in both longitude and grey levels more clearly distinguish the non-RVM features in Fig. 1, largely because the adjacent weaker RVM emission is better delineated. Thus the disparate behaviour of the steep PA-distribution feature can be clearly discerned by simple contrast with the other PPM and SPM emission that shows the usual RVM dependence.

The contrasting RVM and non-RVM aspects of B0329+54’s PA distribution are also clearly seen in ES04’s fig. 1. Their sensitive, well resolved and calibrated 328-MHz observation is directly comparable with Fig. 1 (left) and shows almost identical features. Here, the additional levels of the colour-intensity-coded PA distribution shows the nearly RVM behaviour of the SPM track with exceptional clarity. It is useful to compare how the linear PA ‘‘kink’’ and

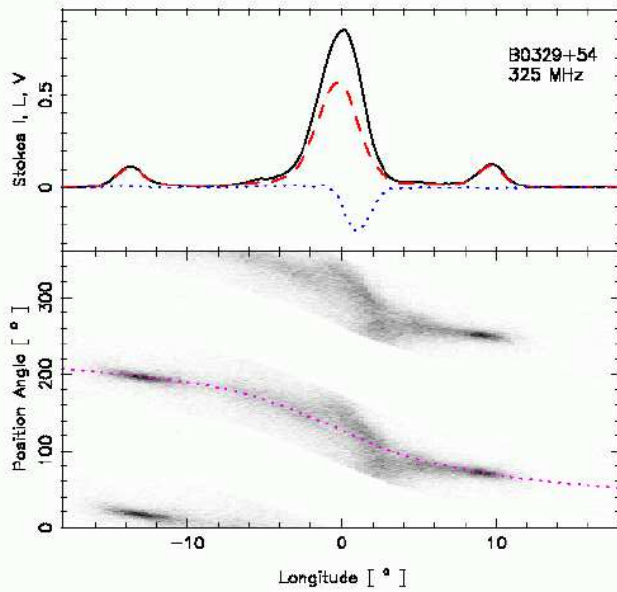
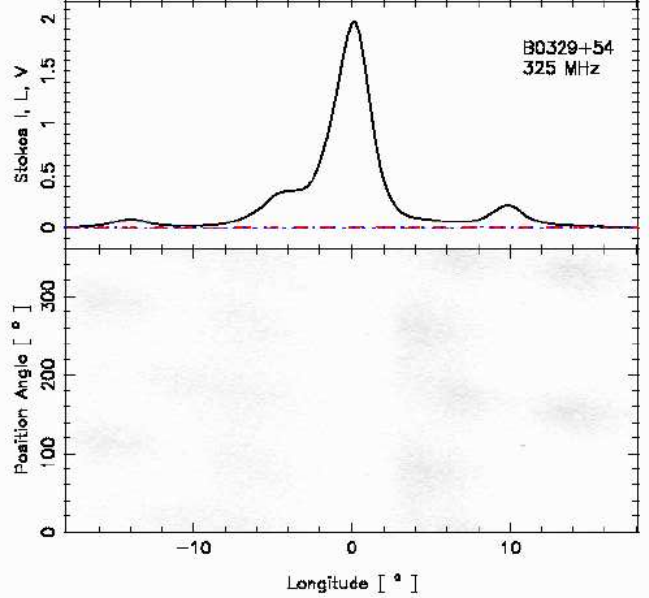
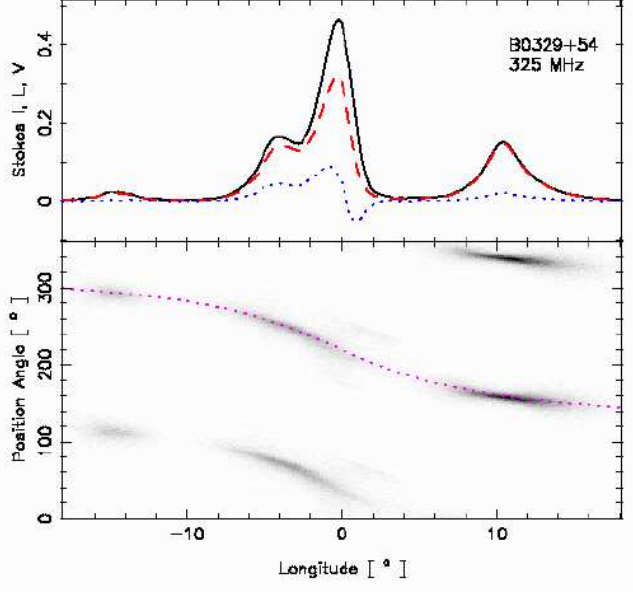


Figure 4. Polarization-mode-segregated PA distributions corresponding to the 325-MHz observation as in Fig. 1, showing the PPM (left), SPM (upper right) and unPOL (bottom) distributions. The peak intensity of the PPM is about twice that of the SPM profile, but the unPOL peak is about twice that of the former—reiterating that subpulses in the central part of the profile are typically less than 40% polarized. Here we see the “pedestal” feature at about -4° longitude prominently in the weaker SPM profile, but its aggregate linear depolarization indicates an equal contribution of power from the strong PPM profile. Note also how completely the unPOL profile has been “cleaned” of polarization.

its canted extending “spot”—making an overall “arc”—are depicted by the grey and colour plotting methods.

Many of the same features can also be seen in SP98’s 103-MHz PA histogram (their fig. 2). The two OPM tracks through both the core and main conal components are clearly evident; the average PA even tracks that at higher frequencies over most of the profile. The signal-to-noise ratio (hereafter S/N) and resolution of the observation is inadequate to fully distinguish the non-RVM emission; the PPM PAs associated with the core component are conflated into an elongated and overexposed spot. However, its elongation on the trailing side to smaller PA values appears to be in just the position of the trailing “spot”.

Remarkably, the 610- (bottom) and 2695-MHz (right) polarisation displays show very similar features: The former is almost identical to the 325-MHz behaviour apart from the much weaker leading-component SPM feature. The characteristics of the PPM emission, both the RVM track and non-RVM “arc” are virtually indistinguishable. What subtle differences there are in the 610-MHz PA distribution are mostly the results of a somewhat reduced S/N. Even at 2.7-GHz the same features are easily recognizable: one model RVM curve passes through the leading PPM feature, just under the steep central “kink,” and then again through the trailing PPM conal “patch”; whereas, the SPM curve passes both through the central and trailing features. The 2.7-GHz



PA distribution thus seems to differ from the others only in subtle aspects.

Focusing on the non-RVM “kink,” a thin dashed line (having a slope of $-21.6^\circ/\circ$) indicates their position consistently at each frequency for convenient comparison. Apart from a more limited extension at 2.7 GHz (which may reflect the poorer S/N), the feature exhibits an essentially identical PA-longitude dependence at each frequency. The same cannot be said for the trailing “spot”; its position appears to shift slightly between 325 and 610 MHz (from about 85° to 78°) and then is seen at a dramatically smaller PA at 2.7 GHz (about 50°).

Overall, we find that both the RVM and non-RVM “kink” emission features in B0329+54’s PA distribution have a broadband nature. We see that the position and slope of the linear “kink” relative to the PPM track is nearly identical at all three frequencies—so that no PA shift is dis-

Table 2. B0329+54 Emission Geometry

Method	α ($^{\circ}$)	β ($^{\circ}$)	Note	Ref
L&M	30.8	2.9		LM88
W_{core}	32	—		R90
ETVI	30	2.1		R93b ^a
PA sweep	59 ± 20	-4.5 ± 2	PPM	GL95
	42 ± 20	-3 ± 2	SPM	
This paper—				
PA sweep	35.5 ± 13	-3.7 ± 1.0	cor 92%	this paper
Thorsett	32.1	-3.38		MR02

^aThis analysis used a steeper average PA sweep rate of $-13.5^{\circ}/\text{degr}$, thus the smaller values of β .

cernible. Only the “kink”’s extension appears to decrease at the higher frequencies, and this may simply be due to the decreased S/N. Note that the average circular polarization below the central component is negative at all frequencies.

IV. INTENSITY DEPENDENCE OF POLARIZATION PROPERTIES

Figure 2 displays a 100-pulse section of the 325-MHz observation in Fig. 1 in full polarisation. Both the strong central feature and weak conal outriders are very apparent, and on closer inspection one can see that the former exhibits a surprising complexity. In certain intervals the central component is so weak that it seems to be undergoing “core nulls”; at other points (*e.g.*, just before pulse 130) it appears double; and when it is emitting most strongly it has a single form that just precedes the longitude origin. On this basis and of course MH93’s work, therefore, we began to wonder whether the non-RVM portion of the central emission participates in the systematic intensity dependence.

A ready means of exploring this question was that of segregating the individual pulses according to their overall intensity relative to the off-pulse noise level. For this we defined a longitude window (-4.13 to $+6.19^{\circ}$) that encompassed the bright central component (III) under which the non-RVM structure is present. We used its total intensity to determine the mean signal-to-noise ratio (S/N) of each pulse within the window and so divide the pulses into respective S/N categories. Thus, the 325-MHz observation was segregated into 15 S/N levels. The lowest level was comprised of 197 pulses and showed no discernible non-RVM effects, whereas the higher S/N levels exhibited increasingly obvious departures from RVM behaviour. A similar separation was possible for the 610-MHz GMRT observation, but at 2695 MHz the overall S/N of the Effelsberg PS was poorer so that the lower intensity effects could not be distinguished well enough to be useful; it was clear however even here that the stronger pulses at this frequency tended to exhibit the non-RVM properties.

We were thus able to distinguish the 2970 325-MHz pulses by their S/N level over the above range, and each of these intensity “bins” was plotted in a manner similar to Fig. 1. Upon inspection of these PA distributions, we found that three distinct kinds of behaviour were seen at S/N levels of unity, up to and around 7, and then around 12—and we then constructed new displays in which the S/N range is

so fractioned. Figure 3 (left, right top and bottom, respectively) then gives these PA distributions.

The S/N “binning” above segregates the PS *entirely* on the basis of central-component strength. Thus the three partial profiles show clearly that the amplitudes of the leading and trailing conal components (I & IV, as well as the core “pedestal”) are largely independent of its intensity variations. The very weakest section (left) exhibits a profile having five clear components, verifying by a new method the longstanding understanding (*e.g.*, Hesse 1973, Kuz’min & Izvekova 1996) that a weak pair of components lies in between the usual four (VI & V, respectively). Here the core “pedestal” at about -4° is almost indistinguishable. More pertinent to our present concern, however, is the remarkably “clean” PA distribution, which clearly defines both the PPM and SPM “tracks” and shows no hint of non-RVM emission.

We see a very different configuration at intermediate intensity levels (Fig. 3, top right): Here the conal outriders have about the same amplitudes (as in the earlier low S/N display), but the bright central component is some 10 times stronger and is preceded by a somewhat weaker “pedestal” feature at about -4° longitude. The aggregate linear polarisation in the central profile region is slight, but Fig. 2 demonstrates that the fractional linear of the individual pulses here often reaches some 50%—thus the PA distributions are very well defined. It is then completely understandable that little aggregate linear survives. We can discern that the “pedestal” feature is characterized by strong SPM as well as PPM power that exhibits an RVM distribution—and its nearly complete depolarization shows that their levels must be about equal. The non-RVM “kink” is situated prominently just adjacent to the PPM track, occurring well on the trailing side of component III. Its steeper linear appearance is familiar from the distributions of Fig. 1, and we note that it just reaches the PPM track on its trailing end. It is also worth noting that the comp. III is labeled (here and in some other partial profiles) by weak anti-symmetric circular polarisation in a core-like manner—and also that the “kink” nearly coincides with the negative (rhc) peak.

Furthermore, the highest intensity pulses (Fig. 3, bottom right) show yet a different behaviour: Here the bright central component (III) is strongest by far—both the “pedestal” as well as the conal outriders retain nearly equal intensities to those seen at lower S/N levels. The SPM track is very similar to that seen at intermediate intensities, but for decreased prominence under both the leading conal component and the trailing half of the central component. The most striking effect here, however, is the shift of the non-RVM “kink” emission to earlier longitudes and the appearance of the trailing “spot.” This surely is very clear evidence of intensity-dependent behaviour.

With regard to the “kink”, the Fig. 3 diagrams do not fully exhibit what is seen in the full set of 15 intensity-segregated profiles (not shown). There, at higher levels, the non-RVM PPM emission consists of two “spots”, the later one whose position is fixed and the earlier one which shifts progressively earlier as the intensity increases. We see this motion of the leading “spot” conflated into the elongated “kink” in the mid- and high intensity panels of Fig. 3 (right top and bottom). The “kink” shifts are not linear (and the dashed line is not a fit, only a reference mark), and seem

to curve slightly along the PPM track, displaced by perhaps some 1.5° ; and the 325-MHz “spot” lies below the PPM track by a roughly similar amount. The “spot” is associated with the far trailing edge of the central component, which is almost fully right-hand circularly polarized (something also very clearly seen in ES04’s fig. 1). This easy to miss circumstance now prompts interest in the leading portion of the central component where left-handed circular power is often seen, but has disappeared in this average of very bright individual pulses. The dynamics of this averaging is very clearly shown in the bottom panel of ES04’s fig. 1, where the canted band shows how the circular polarization depends on longitude—and the leading “spot” motion above then links higher intensity levels with increasing LH circular polarization (see also Fig.5).

In summary, Figs. 1–3 show in different ways that both polarisation modes exhibit an RVM behaviour with almost continuous tracks at all longitudes—that is, the non-RVM power associated with the PPM is seen in addition to a clear RVM track. Only at the highest intensity levels do the PA distributions suggest that non-RVM emission may displace the RVM emission in certain longitude regions under the central component.

The SPM, however, seems to span a larger pulse-longitude range than the PPM (see also, GL95: fig. 1, SP98: fig.2; and ES: fig. 1). We have segregated the modal power using the three-way method described in Deshpande & Rankin (2001; Appendix), which produces PPM, SPM and unpolarised (unPOL) PSs. In this method the modal power of each sample is given to either the PPM or SPM PS and the unpolarised power to the unPOL PS. Partial profiles corresponding to these fractions of the total PS are shown in Figure 4, where we see that the peak intensity of the unPOL profile (lower right) is about twice that of the PPM profile (right); moreover, the SPM peak is about 40% that of the PPM peak. Note also that the PPM and SPM PA traverses follow the RVM rather well even in regions close to the central component; the only serious departures are the “kink” and the “spot” under the latter part of the PPM component III.

We have also segregated the modal power into a pair of PPM and SPM PSs using the two-way method which is also described in the above Appendix. This method makes the further assumption that all of the depolarisation follows from the interference of two fully polarized intrinsic basis modes. The overall results obtained with this second method differ rather little from those above. The PPM and SPM PA distributions are nearly identical to those seen in the first two panels of Fig. 4—the primary difference being that the large amount of depolarized power (seen in the unPOL panel) is now folded into the PPM and SPM PSs. Indeed, there is still approximately a factor of two power difference between the two segregated modal profiles. Overall, then, these results appear compatible with the premise that most of B0329+54’s depolarised power does stem from the incoherent superposition of PPM and SPM radiation.

V. INTENSITY DEPENDENCE OF THE BRIGHT CENTRAL COMPONENT (III) AND ITS NEIGHBORS

Sets of 4 intensity-fractionated profiles are given in Figure 5 for the PPM, SPM and unPOL partial PSs, and their three panels depict the total power, total linear and circular polarisation. The PPM (left) central component is nearly unimodal, whereas that of the SPM (top right) is, as usual, accompanied prominently by the “pedestal” feature. In each of the displays the profiles corresponding to the four intensity fractions overlap each other, but can readily be identified by their increasing amplitudes. All three displays show the intensity-dependent character of component III: this effect is seen strongly in the PPM and unPOL (bottom) plots, but is also discernible in the SPM plot. The PPM total power peak shifts from about $+0.5^\circ$ in the least intense fraction to some -0.5° at the largest intensities, a larger effect by nearly twice than reported by MH93 for the total profile. The unPOL profiles also show a dramatic effect, but here we see a progressive motion on the leading side of the feature and near stasis on the trailing side—such that the high intensity features are broader. The weaker SPM with its “pedestal” feature generally peaks somewhat earlier and exhibits the least retardation with intensity.

These circumstances suggest a very different, more dynamical way of understanding the complex shape of B0329+54’s central component. At the lowest intensities, we saw that the central peak falls at positive longitude (see Fig. 3, left) and shows a larger half-power width than at higher intensities. At intermediate and higher intensities the PPM power moves strongly earlier, and at the highest intensities shows the sharp rise and quasi-exponential fall-off seen in Fig. 5 (left). This most intense PPM power together with the more symmetric unPOL power, dominates the total profile form, especially on its leading edge, and tends to narrow its overall width. Indeed, measurement of the entire set of 15 intensity-fractionated profiles computed from the total PS shows that the trailing half-power point of the central component moves earlier by fully 1.5° .¹

Perhaps, we should regard the B0329+54’s central component as an incompletely illuminated core component. This begs the question, however, about why some of this core’s emission is both narrower in width and so conspicuously dependent positionally on its intensity. It is worth noting that the most intense PPM profile in Fig. 5 exhibits a nearly antisymmetric circularly polarised signature whose center falls at the longitude origin, whereas most of its emission precedes this point. Thus the radiation on the trailing side of this high intensity PPM emission is largely or completely right-hand circularly polarized (as seen in ES04). And this is just the position of the non-RVM “kink” and “spot.”

We note with interest that the overall normal mode core (III) exhibits a similar shift to earlier longitude with respect to its abnormal mode position. This fact can be seen clearly in both BMSH: fig. 3 and SP02: fig. 1, showing that over a remarkably large band the normal mode core is emitted about $\frac{1}{2}^\circ$ earlier than its abnormal mode counterpart. Al-

¹ Note that the intensity-dependent shift of the core peak is just barely discernible in Fig.3, because too many intensity levels are conflated.

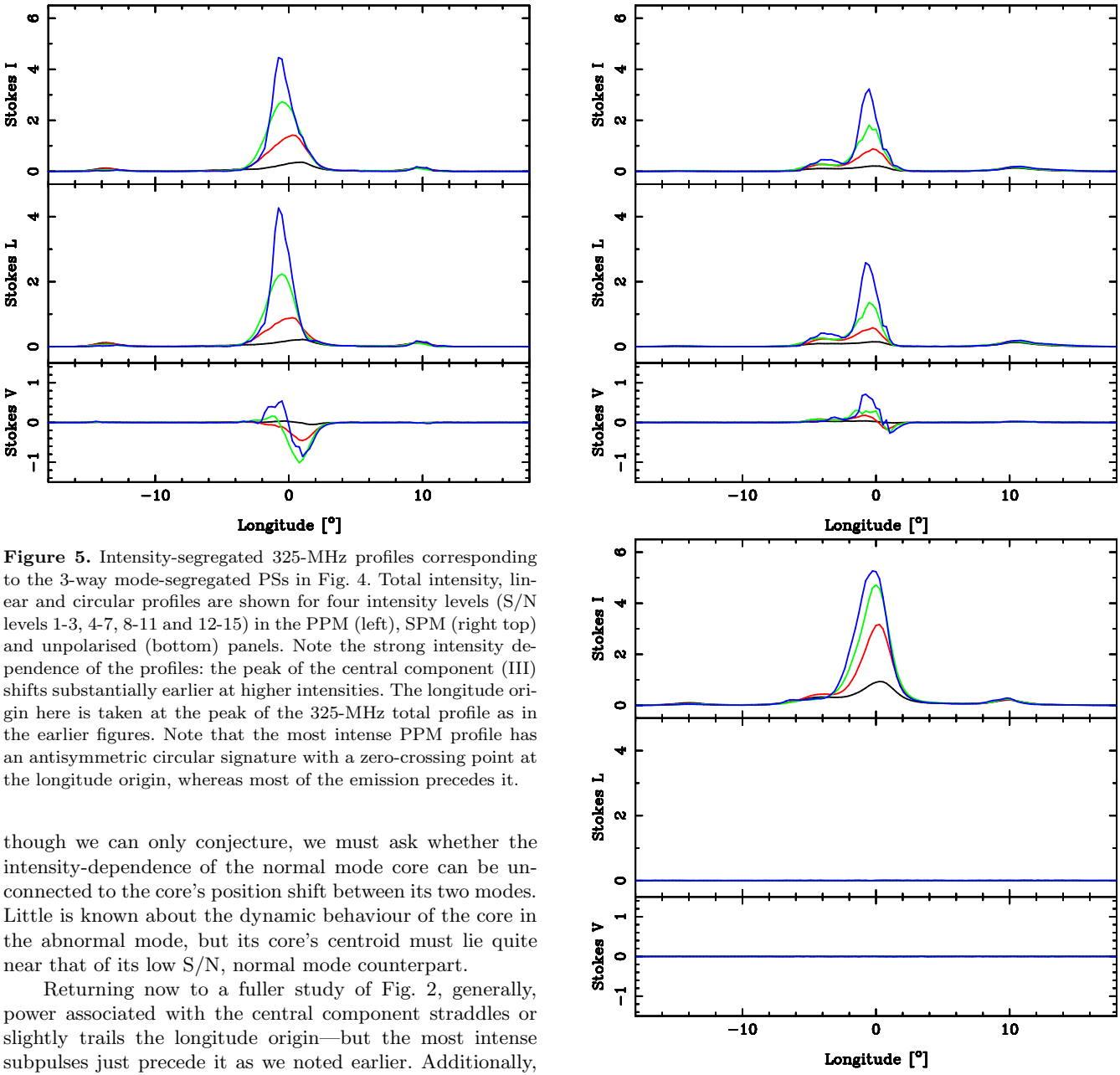


Figure 5. Intensity-segregated 325-MHz profiles corresponding to the 3-way mode-segregated PSs in Fig. 4. Total intensity, linear and circular profiles are shown for four intensity levels (S/N levels 1-3, 4-7, 8-11 and 12-15) in the PPM (left), SPM (right top) and unpolarised (bottom) panels. Note the strong intensity dependence of the profiles: the peak of the central component (III) shifts substantially earlier at higher intensities. The longitude origin here is taken at the peak of the 325-MHz total profile as in the earlier figures. Note that the most intense PPM profile has an antisymmetric circular signature with a zero-crossing point at the longitude origin, whereas most of the emission precedes it.

though we can only conjecture, we must ask whether the intensity-dependence of the normal mode core can be unconnected to the core's position shift between its two modes. Little is known about the dynamic behaviour of the core in the abnormal mode, but its core's centroid must lie quite near that of its low S/N, normal mode counterpart.

Returning now to a fuller study of Fig. 2, generally, power associated with the central component straddles or slightly trails the longitude origin—but the most intense subpulses just precede it as we noted earlier. Additionally, “pedestal” emission can be seen at about -4° longitude in many pulses, often giving the impression that the “core” is double. The linear and circular polarisation in this central region is not small, the former typically some 50% (green) but reaching 70% (yellow). Left-hand circular predominates prior to the longitude origin and right-hand after it, both at typical levels of 40%. Given the slight polarisation of the total profile (see Fig. 1), it is clear that both OPMs are active throughout this central region. Nonetheless, the PA distribution in Fig. 2 indicates that PPM power (magenta) tends to predominate on the leading side of the origin and SPM power (cyan) just after it, but the pronounced stripes of low linear polarization (blue colour) in the second column give some indication of how the depolarisation occurs.

We must distinguish carefully between the various contributions to the power on the far leading side of the central component. In the total profiles of Fig. 1 this is the region of the “pedestal”, but in the colour display we can see that

much of this power consists of a distinct component at some -4° longitude. Given that individual subpulses can be found at almost any longitude in the -5 to -2° range, one can justly doubt whether this power comprises an actual component, but note that we see the feature clearly at intermediate intensities (Fig. 3, top right) and in the SPM profiles of Figs. 4 & 5 (both top right). Moreover, the nearly complete depolarization at this longitude in the total profile indicates that PPM power accrues at a similar level and form.

Conversely, we emphasize that this feature at -4° longitude contributes most of the power to the “pedestal” seen in G&G's fig. 1 as well as our Fig. 1 above. This issue is important, because G&G do not count this feature among their well known 9. Evidence of power at -4° can be seen clearly in several of their partial profiles shown in their fig. 3 (and then averaged in the lower panels—but note carefully that these are not total average profiles!), but it never breaks out

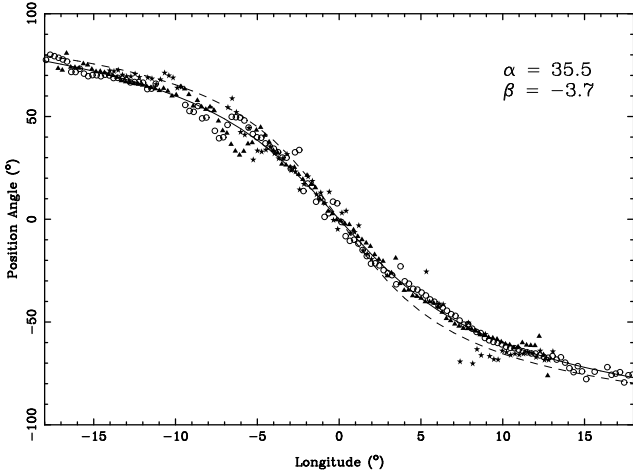


Figure 6. RVM fits to the PA traverses. The 325-MHz data of S/N 1 PPM (filled triangle) and SPM (open circle) PA values obtained from the data of Fig. 3. Each of the tracks were fitted separately and then aligned. The full line is the RVM fit to these combined tracks. The 610-MHz SPM (asterisk) values pertain to the lowest S/N 1 profile (of 7); a fit was used to determine its inflection (steepest gradient) point and then to align it with the other curves. We see here that the PA traverse is largely independent of frequency. The dashed line corresponds to the average α and β values of 51° and -4° reported by GL95, which is here clearly seen to deviate from our measured values.

into a separate feature in their total-power analysis. G&G do identify a new feature just a little earlier, at -5.5° , which they denote as comp. II—and we see very occasional weak subpulses in Fig. 2 which may correspond to it (*e.g.*, pulse 102). This comp. II, however, does not substantially contribute to the total profile “pedestal” (apart, perhaps from extending its early edge), and so again G&G’s comp. II and the “pedestal” component at -4° longitude are entirely distinct entities. We refer to this feature at -4° longitude as component X.

Fig. 2 also shows occasional weak subpulses at about $+4.5^\circ$ that apparently correspond to G&G’s comp. V (*i.e.*, pulse #120) as well as some few others at the $+6.9^\circ$ longitude of their comp. VII (*i.e.*, #193). There is no very good example in this colour display of G&G’s comp. VI at -9.5° (except perhaps #184). Subpulses associated with the bright conal components (I and IV) are very clear in total power, but display a complex behaviour in linear polarisation. Broad, low level SPM emission is splayed within and outside the regions occupied by these components (red-orange angles at negative longitudes and chartreuse colour at positive ones); whereas the the bright subpulses (cyan and purple angles, respectively) tend to be PPM dominated and are more closely aligned with the component centres.

We have computed the auto-correlations (ACFs) and cross-correlations (CCFs) of both the natural 325-MHz PS as well as of the 2- and 3-way segregated PPM and SPM PSs. Generally, the ACFs at zero delay show a diagonal line of complete correlation as well as symmetrical off-diagonal “knots” of local correlation associated with distinct components—and a number are seen, confirming G&G’s finding that the pulsar’s emission is comprised of multiple components. These ACFs, however, indicate no zero-delay correlation between any of the components, and in partic-

ular complete independence between fluctuations of the -4° “pedestal” and central component, even in the SPM. This surely establishes that B0329+54’s leading “pedestal” is an independent emission feature, and we can question whether it is more core- or cone-like, or neither. Further, it indicates that the core’s leading “gouge” is a part of its structure, not a result of “absorption”. CCFs between the two OPM PSs at zero delay suggest possible propagation delays between the two contributions to core power—again of the order of $\frac{1}{2}^\circ$ longitude—and CCFs at ± 1 period delay show significant (typically 30%) asymmetric correlation between different parts of the core component.

VI. EMISSION GEOMETRY

Sightline and Conal Beam Geometry

Pulsar profiles provide fundamental information about pulsar beamforms and emission geometry, and B0329+54’s overall triple profile form has long been taken as strong evidence for a core-cone beam configuration (Backer 1976). We do not understand the physical origins or all of the implications of this circumstance, but in reviewing many studies of PSR B0329+54 bearing on this interpretation, we now find a large body of detailed analysis which supports it.

B0329+54 has a core-cone (Lyne & Manchester 1988; LM88) triple (T) profile (R83a), and its core and main conal component (I & IV) pair are seen over most of the about 0.06 to 15-GHz band in which it can be detected. Three main lines of evidence furthermore indicate that this pulsar’s conal components represent an outer cone: a) it has another set of weak components in between the major ones [Hesse 1973; Kuz’min & Izvekova 1996; see also Fig. 3 (left)], b) the cone size increases strongly at low frequency (Mitra & Rankin 2002; hereafter MR02), and the OPM configuration and depolarisation (*e.g.*, Figs. 1–3) is typical of outer cones (Rankin & Ramachandran 2003).

Outer cones are known to have particular dimensions relative to the polar cap size (Rankin 1993a,b; hereafter R93a,b). Its outer cone width together with its central PA sweep rate can be used to determine both its magnetic latitude α and sightline impact angle β . Several other methods have also been used to estimate these basic parameters for B0329+54, including those of LM88, direct PA sweep fitting (GL95), the core-width method (R90), and a “Thorsett”-function analysis [see DR01, table 2 for a B0943+10 example or Rankin *et al* (2006), table 2 for B0809+74]—and the results of these analyses are given in Table 2.

We have carried out our own analyses by fitting the PA traverses of the 325- and 610-MHz observations. Noting that the 325-MHz S/N-1 modal PA tracks as seen in Figure 3 are not corrupted by major non-RVM features, we have fitted the PA track of each mode to eq.(1) according to the injunctions of Everett & Weisberg (2001) and Dyks *et al* (2004). Further we fitted the RVM to the 610-MHz S/N-1 (out of 7) SPM PAs which showed a clean RVM PA track. These three fits yielded mutually consistent α and β values. The fiducial longitudes obtained for each of these fits were used to overlay the three sets of PA values as shown in Figure 6. The combined PAs were then again fitted to eq.(1), and the results are summarized in Table 2. As expected this analysis

showed high correlations between α and β , thus the large errors— 35.5 ± 13 and $-3.7 \pm 1.0^\circ$, respectively. The fiducial longitude, was well determined at $+0.3 \pm 0.5^\circ$ relative to the peak of the central component in an overall average profile.

Table 2 exhibits that all the available analyses result in similar, and generally compatible, estimates for B0329+54's magnetic latitude α and sightline-impact angle β . The older analyses tended to use larger values of the central PA sweep rate R , because the different OPM behaviours were then unknown. Larger errors are expected from methods which directly fit the PA traverse (and use no profile-width information), because α and β are highly correlated in eq.(1)—as we found above. Given the coherence of these analyses (as well as the weight of the many similar analyses applied to many other pulsars which vet and calibrate them), we must conclude that B0329+54's magnetic latitude is in the $30\text{--}35^\circ$ range and probably near 32° . Furthermore, its β is near -3.5° , and the negative sense (poleward sightline traverse) is indicated by a significantly better goodness of fit.

In addition to B0329+54's outer conal components (I & IV) and the long known other ones (II, V & VI), (G&G) identified three additional components and argued that they represented four concentric cones of emission—one pair outside the outer conal set and two other pairs within (This innermost pair can apparently be seen as minor inflections at -5.5 and $+4.5^\circ$ in the PPM partial profile of Fig. 4, left). They then carried out an A/R analysis to compute their emission heights, using the central core component as the reference longitude. Though the other inner component pair is too weak to show in the average profile, our analysis above does tend to confirm them. Also, our computation of the PA-traverse center above makes it possible to apply Blaskiewicz *et al's* (1991) method directly. The results of this procedure would, however, provide only a small correction to those of G&G, given that the PA inflection lags the normal-mode core peak only slightly.

Core Emission Geometry

The implication of these largely conal analyses is that B0329+54 has an angular polar-cap diameter of some $2.45^\circ P_1^{-1/2}$ or 2.9° , where P_1 is its rotational period of 0.7145 s and moreover that for an α of about 32° , we should expect a core-component width $2.45^\circ P_1^{-1/2} \csc \alpha$ of about 5.5° longitude. This line of argument has itself been used to determine α for many pulsars (R90) and the resulting values in turn found to agree very substantially with LM88's method (Bhattacharya & van den Heuvel 1991).

Nominally, the core-width estimate has been found to agree best with measurements at around 1 GHz as the core components of most objects tend to become broader at lower frequencies (Rankin 1983b; hereafter B83b). For B0329+54 measurements show observed normal mode core widths in excess of 4° in the 1–2 GHz band, possibly up from some 3.8° at 15 GHz. The high quality observations of von Hoensbroech & Xilouris (1997) show a symmetrical, Gaussian-shaped core component at 10.55 GHz, but ever more asymmetric “notched” forms at longer wavelengths: at 4.85 GHz their core is just perceptibly canted on its leading edge with a 4.4° width, whereas at all lower frequencies down to our own 610- and 325-MHz observations, the size of the “gouged” leading region of the core component increases.

This is particularly clear in Fig. 1 (right) at 2.7 GHz, where we see a clearly asymmetric core component in which a double inflection on its leading edge suggests a missing portion. Also note that the leading “notch” is progressively deeper at 610 (bottom left), at 325 MHz (top left) and at 103/111 MHz (see SP98: fig. 4). Around 100 MHz the intrinsic core width is some 3.5° and corrected values appear to vary little down to 61 MHz (Suleymanova 2006).

The strange shape and spectral changes of B0329+54's bright central region, we have seen above, have several causes. First, it is comprised not only of the core component (III) but also the “pedestal” feature, which in turn is comprised mostly of comp. X but also G&G's comp. II. Comp. III, however, surely appears to be the core component. Its antisymmetric circular polarization, when present [*e.g.*, in the SPM, Fig. 4 (top right)] tends to have a zero-crossing point near the longitude origin taken at the peak of the central component—and we have also seen that this aligns closely with the PA inflection point. Second, the core-component width falls short of the 5.5° polar cap diameter, thus it does appear to be only partially illuminated. However, this total profile width is dominated by the bright, narrow, earlier-shifting PPM SPs, again contributing to the core's canted shape. It is worth noting that the core's width in the average of the weakest pulses (see Fig. 3, left) could be nearly that of the polar cap. Therefore, we have no basis for regarding the “pedestal” and component III together as a “notched” (or “absorbed”) core component (this line of interpretation was taken in R90). And perhaps B0329+54 can give guidance regarding the other stars having seemingly “incomplete” cores with a bright trailing and weaker leading portion [*e.g.*, Srostlik & Rankin (2005) were able to show that a very comparable situation obtains for pulsar B1237+25].

VII. SYNTHETIC ANALYSIS & DISCUSSION

In the foregoing sections we have reported on our detailed analysis of three exceptionally high quality observations of pulsar B0329+54, two made with the GMRT at 325 and 610 MHz, and a third from the Effelsberg Telescope at 2.7 GHz. Many studies of this pulsar are available in the literature—a number of which we have reviewed in the Introduction—but few attempt to delineate the properties of the star's central core component. By contrast, we take this central component as our main interest. We discover that the pulsar's polarisation properties are strongly dependent on the intensity of the core emission. At lower core intensities, the PA behaviour is largely consistent with the RVM, which allows us to pursue a model for the pulsar's emission geometry.

Absolute OPM Orientation

As was well established earlier by BMSH, GL95, Mitra (1999) and ES04, the two OPMs can be traced throughout most of B0329+54's profile. Following current practice, we have taken the stronger mode as the PPM (*e.g.*, Fig. 1, top left). However, this delineation of the OPMs is no longer adequate. We require a physical or fundamental geometrical basis for distinguishing between the two OPMs, and the well measured proper motion of Brisken *et al* (2002) together

with the absolute polarimetry of Morris *et al* (1979) provides such a means.

Recently, Johnston *et al* (2006) have revisited the question of whether pulsar rotation axes are aligned with their proper-motion directions, making a good case that the natal supernova “kick” is either parallel or perpendicular to the rotation axis. Part of this latter uncertainty follows from our ignorance about the orientation of a specific OPM with respect to the projected magnetic field direction. One of us (Rankin 2007) has checked and extended the above work and confirms that the case for the star’s rotation axis to be fixed relative to the supernova kick direction is indeed very strong. Further evidence for such alignment is seen from the x-ray observations of young pulsars (Helfand, Gotthelf & Helpman 2001, Ng & Romani 2004).

For B0329+54, Morris *et al* determined that the absolute PA (measured ccw from north on the sky) at the peak of the central profile component was $19 \pm 4^\circ$. The value, based on the observations in Morris *et al* (1981) at both 1.72 and 2.69 GHz and a correct rotation measure, is as accurate as can be obtained with average polarization. We have checked these calculations carefully, and used our observations to confirm the relationship between the average and RVM “track” PAs. Brisken *et al* measure B0329+54’s proper-motion direction (again ccw from north on the sky) as $119^\circ \pm 1^\circ$. The difference angle Ψ ($=PA_v - PA_o$) is then $100^\circ \pm 4^\circ$. The average PA at the fiducial longitude is distorted by the PPM “kink”, thus Morris *et al*’s PA_o value probably exceeds the RVM PPM by $5\text{--}10^\circ$. Nonetheless, we find that the pulsar’s PPM polarization is nearly orthogonal to the projected magnetic field direction.

We reemphasize that the above value applies to the PPM. If the star’s natal “kick” was delivered parallel to its rotation axis, then this identifies the PPM as the OPM orthogonal to the projected magnetic field direction. In their theory of magnetospheric wave propagation, Barnard & Arons (1986) identify the wave polarized perpendicular to the projected field direction as the extraordinary (X) mode; thus the PPM (solid curve) in Figs. 1, 2 and 4 can be associated with the X mode and the SPM with the ordinary (O) mode.

This identification of the SPM with the O propagation mode apparently makes this mode subject to refraction; whereas, the X mode propagates in a manner independent of refraction. Furthermore, the refraction direction is expected to be outward, towards the conal edges (Barnard & Arons 1986, Lyubarskii & Petrova 1997, Weltevrede *et al* 2005)—that is, outward with respect to the magnetic axis—and the PPM/X is the inner of the two modes under the main conal components. Thus, if both conal OPMs arise in the same region,² we should expect the O-mode emission to have been refracted outward relative to that of the X mode. This behaviour of the outer conal components is very usual as we had noted above (Rankin & Ramachandran 2003),

² Our observation seems to show good evidence that the two modes are indeed arising from the same height. We find that for the mode-segregated PPM and SPM, the center of the outer conal outriders leads the steepest gradient point by about 2° . By applying the BCW model this give an emission height of about 300 km for both the modes. However, even better S/N than what we have is needed to establish this fact with certainty.

and differences in the directions of X- and O-mode propagation may provide a direct measure of the magnetospheric refraction in peripheral regions of a pulsar’s polar flux tube. Finally, the circumstance that the identified O mode is the outer conal emission mode lends support to the premise that B0329+54’s supernova “kick” was indeed aligned with its rotation axis.

Much is yet to be learned about the conal structure of this pulsar and its causes. While two emission cones are well known in a number of pulsars, only for B0329+54 is there evidence for four (G&G). In addition to the bright third cone (comps. I & IV), we confirm the innermost cone comprised of G&G comps. II and V and also find that it is PPM (X-mode) dominated (*i.e.*, Figs. 3, 4, left). Regarding G&G’s second and fourth cones, our generally core-directed analyses resulted only in the detection of a few weak sub-pulses at the specified longitudes, so insufficient to serve as confirmation.

A Glimpse of the Polar-Cap Acceleration Process

Turning now to the perplexing PA “kink” in the pulsar’s PPM traverse, we recall that it a) extends across much of the star’s core component; b) is associated with a strong intensity-dependent shift of the core’s position to earlier longitude; and c) is highly right-hand (negatively) circularly polarised at low intensities, but gradually shifts to $+/$ -anti-symmetric circular at high intensities. Each of these properties is well demonstrated by our analyses above. And we reemphasize that the “kink” is a frequency-independent feature: slightly different parts of it are revealed at the three frequencies (with their particular S/N levels)—and different parts of it clearly correspond to different intensity levels—but the feature as a whole exhibits a single consistent PA-longitude dependence.

The identification of the PPM “kink” with the X mode, as demonstrated in the previous section, rules out propagation effects as its primary cause. Other possible grounds dismissing propagation effects hinge on the “kinks” complete constancy over a three-octave frequency band. We must then understand the “kink” emission as reflecting an unusual viewing or emission geometry. We also assume that B0329+54’s magnetic field is nearly dipolar. Consequently, the “kink” indicates high altitude emission largely along the magnetic axis. However, were this occurring at a fixed altitude, we would see a different sort of “kink”, one with a fixed longitude displacement from the PPM track. But in fact, the steeper PA track of the “kink” indicates that its longitude displacement (from the RVM “track”) increases from zero to some 1.5° or so over precisely the same longitude interval in which the intensity-dependent shift of the PPM core emission is observed. This is just the signature of a height-dependent amplification or cascade: the weaker core emission is emitted at low altitude and, as its intensity increases, so does its emission height. These various circumstances are clearly indicated in Figs. 1, 2 and 4.

We then have two ways of using the combined effects of A/R to estimate the range of emission heights over which this cascade or amplification process occurs: we can measure the maximum longitude displacement of the “kink” from the PPM RVM, or we can directly estimate the time interval corresponding to the range of height-dependent retardation

observed in the core emission. Neither is trivial to measure precisely,³ but both represent shifts of roughly 1.5° longitude. The displacements are both produced equally by the aberration and retardation, so only half of the shift is associated with the retardation and thus the emission-height difference. 1.5° then corresponds to 3 ms, and half of this to a height difference of some 450 km (Dyks *et al* 2004).

Finally, let us consider the circular polarization. Figs. 4 and 5 indicate that Stokes V is $+/-(lh/rh)$ antisymmetric both in the SPM and in the PPM at high intensity; at low intensity the PPM peak falls after the longitude origin and is negatively circularly polarized. So, we see that the intense PPM emission largely fills the polar cap region and exhibits the antisymmetric circular-polarization signature frequently seen in core features. Moreover, its $+/-(lh/rh)$ sense and clockwise-rotating PA is expected if the polar cap region is longitudinally extended (Radhakrishnan & Rankin 1993).⁴

Emission associated with the “kink” then, appears to provide a rare glimpse of the core radiation process. It reveals what seems to be a height-dependent amplification or cascade that moves nearly along the magnetic axis, growing ever more intense with altitude. ES and several other authors (Petrova 2006a,b; Melrose *et al* 2006) have tended to interpret the non-RVM emission and prominent circular polarization in the B0329+54 core as evidence of propagation effects. But we now see that this cannot be so. Both the association of the PPM with the X mode and the broadband nature of the “kink” rules strongly against propagation. Moreover, ES and the others fail to appreciate the primary importance of the intensity dependence (MH93) in their interpretations of this pulsar’s “kink” radiation.

The Perplexing Moving “Spot”

In contrast to the “kink”, the spot appears to show a strong movement with frequency. Its behaviour can be traced through the three panels of Fig. 1, where we see it centred at about 2.2° longitude, but appearing at $80-90^\circ$ PA at 325-610 MHz and then some 50° at 2.7 GHz. The “spot” is very clearly associated only with the most intense pulses as is clear from Fig. 3. A less sensitive 21-cm observation (not shown) shows a “track” of PAs something like that seen in the 2.7-GHz panel of Fig. 1 but without the “spot”, so it is important to further explore this possibly very important detailed behaviour. If a systematic motion of the “spot”’s PA and its dependence with frequency can be verified then it could serve as a diagnostic for studying propagation effects in the pulsar magnetosphere.

The Mysterious Component X

A very important question, which our analyses have pointed strongly, is the nature of comp. X. It is the major part of the “core pedestal” and peaks very close to -4° longitude

(whereas G&G’s comp. II is at -5.5°). We see in the figures above (especially Fig. 4, top right) that comp. X is prominent in the weaker SPM, but its nearly complete aggregate depolarisation (see Fig. 1) clearly indicates that it must be comprised of a comparable amount of PPM power. Comp. X appears as companion to the core component, but we find no evidence for any correlated power between it and the core. Its intensity behaves more like the conal components; if it participates at all in the core’s intensity dependence (Fig. 5), it does so in a much weaker manner.

The importance of understanding comp. X is not confined to B0329+54 as a number of other pulsars have similar features. An excellent example is that of B1859+03 at 21 cms (see Radhakrishnan & Rankin 1990: fig. 1), where we see a fully depolarised component prior to the star’s core that is prominently marked by an antisymmetric circularly polarised signature. This leading feature as well as component X appears to be almost fully depolarised over its entire width, and this is unlike what is seen in outer conal components where the PPM and SPM contributions are characteristically displaced somewhat in radius and thus in longitude (Rankin & Ramachandran 2003). Petrova (2000) and Weltevrede *et al* (2005), argue that conal emission can be refracted inward due to assumed lower plasma densities near the magnetic axis, perhaps explaining such a feature; apparently, however, only the O mode would be so refracted, so it is difficult to see how this could be squared with the depolarization of component X.

Concluding Comments

In the foregoing sections of the paper we focussed on the nature of B0329+54’s core component and in particular its non-RVM PA “kink” feature. We find that this feature, which is prominently associated with the PPM, is comprised primarily of X-mode radiation—that is, emission whose electric vector is oriented perpendicular to the projected magnetic field direction. Furthermore the constancy of the “kink” over a wide frequency band rules out the possibility that the effect is due to magnetospheric refraction. Rather, we find that the “kink” must be interpreted in a manner reflecting the geometrical exigencies of the emission processes—primarily aberration and retardation. On the other hand we see what appears to be strong evidence for magnetospheric refraction in the outer conal components. The association of the O mode with the SPM suggests that this mode should be refracted outward, and its broader longitude extent appears to bear this out. The moving “spot” and the X component could also be effects of magnetospheric propagation.

Three key circumstances must be considered in interpreting this “kink” emission: a) its prominent intensity dependence first noted by MH93, and the manner in which the linear polarization of the core emission, increasingly retarded with intensity, produces the “kink”; b) the broadband nature of the “kink” radiation and c) the character of its circular polarization, which is both broadband in character and apparently geometrical in origin. When considered together, the “kink”’s properties appear to provide a rare glimpse of the core emission process, perhaps a cascade or height-dependent amplification.

Core emission has heretofore been inadequately understood, and we hope that these analyses will provide some

³ In particular, we cannot simply measure the “kink” displacement relative to the PPM RVM along a particular PA, because these points represent different longitudes and thus different sections of the field above the polar cap.

⁴ Thomas & Gangadhara (2007) show that this same correlation is expected geometrically from a circularly symmetrical polar cap.

insights which can assist in giving it an improved physical foundation. Given that we now know that ions can be pulled off the surface, it is possible the “kink cascade” can be interpreted in terms of Cheng & Ruderman’s (1980) ion-outflow model where the intensity-dependence of the core would result from increased ionic discharge from the neutron star’s surface. We note that MH93 interpreted the intensity dependence in terms of this model, where the higher intensity of the core could result from increased ionic discharge from the neutron star’s surface. The retardation could then be explained, they argue, as a) an A/R effect due to changes of the emission height or b) due to lateral movement of the core-emission region as a function of intensity. While the ion-discharge might be the origin of the non-linearity behind the intensity dependence, these models provide no further insight into how it is linked to the non-RVM linear or circular polarisation. We have considered the possibility that height dependent A/R effect can give rise to the observed “kink”. However, other possibilities like the ion flow within the polar flux tube might conceivably produce currents which would in turn distort the local magnetic field direction and hence the character of the emitted linear and circular polarisation. Overall, it is difficult to understand why the non-RVM effects are associated only with a single (PPM/X) mode. If the OPMs were produced by two different charged species as proposed by Gangadhara (1995)—then only that one responsible for the PPM might vary significantly in order to distort the PA traverse. However, these and some other suggestions which were reviewed in the Introduction (Gil & Lyne 1995; Mitra *et al* 2000; Mitra & Seiradakis 2004), all ostensibly fail to provide as full an explanation as is needed.

ACKNOWLEDGMENTS

We thank J. Dyks, R.T. Gangadhara, S.A. Suleymanova and G.A.W. Wright for informative discussions and/or critical readings of the manuscript and the GMRT operational staff for observing support. DM would like to thank Alexis von Hoensbroech for providing the 2.7-GHz single pulse data used in this work and which was also used in Mitra (1999) and Mitra *et al* (2000). We also gratefully acknowledge our use of this archival observations from the Effelsberg Radio Observatory courtesy of the Max-Planck Institut für Radioastronomie in Bonn. Portions of this work were carried out with support from US NSF Grants AST 99-87654 and 00-98685. This work made use of the NASA ADS system.

REFERENCES

Backer D.C. 1976, *Ap.J.*, 209, 895
 Backer D.C., & Rankin, J.M. 1980, *Ap.J.Supp.*, 42, 143
 Barnard, J. J. & Arons, J. 1986, *Ap.J.*, 302, 138
 Bartel N., Morris D., Sieber W., Hankins T.H. 1982, *Ap.J.*, 258, 776
 Bhattacharya, D. & van den Heuvel, E.P.J. 1991, *Physics Reports*, 203, 1-124
 Blaskiewicz, M., Cordes, J.M., & Wassermann, I. 1991 *Ap.J.*, 370 643.
 Brisken, W. F., Benson, J. M., Goss, W. M., & Thorsett, S. E. 2002, *Ap.J.*, 571, 906.

Cheng, A. F. & Ruderman, M. A. 1980, *Ap.J.*, 235, 576
 Cole, T.W., & Pilkington, J. D. H. 1968, *Nature*, 219, 574.
 Deshpande, A.A. & Rankin, J.M. 1999, *Ap.J.*, 524, 1008
 Deshpande, A.A. & Rankin, J.M. 2001, *M.N.R.A.S.*, 322, 438
 Dyks, J., Rudak, B., & Harding, A.K. 2004, *Ap.J.*, 607, 939
 Edwards, R.T., & Stappers, B.W. 2004, *A&A*, 421, 681 (ES04).
 Everett, J. E., & Weisberg, J. M. 2001, *Ap.J.*, 553, 341.
 Gangadhara, R. T. 1995, *Ap&SS*, 232, 327.
 Gangadhara R.T., Gupta Y. 2001, *Ap.J.*, 555, 31(G&G)
 Gil, J. A., Lyne, A. G., Rankin, J. M., Snakowski, J. M., & Stinebring, D. R. 1992, *A&A*, 255, 181.
 Gil, J. A., & Lyne, A. G. 1995, *M.N.R.A.S.*, 276, 55.
 Gould, D.M., & Lyne, A.G. 1998, *M.N.R.A.S.*, 301, 253.
 Gupta, Y.; Gothoskar, P., Joshi, B. C., Vivekanand, M.; Swain, R., Sirothia, S.& Bhat, N. D. R., 2000, *ASP Conf. Ser.* 202: IAU Colloq. 177: Pulsar Astronomy - 2000 and Beyond, 227
 Hankins T.H., & Rankin, J.M. 2006, *A.J.*, submitted
 Helfand, D. J., Gotthelf, E. V.& Halpern, J. P. 2001, *Ap.J.*, 556, 380
 Hesse, K. H. 1973, *A&A*, 27, 373
 von Hoensbroech, A., & Xilouris, K.M. 1997, *A&A Suppl.*, 126, 121.
 von Hoensbroech, A. 1999, Ph.D. Thesis, Bonn University, Bonn, Germany.
 Hobbs, G., Lorimer, D. R., Lyne, A. G., & Kramer, M. 2005, *M.N.R.A.S.*, 360, 974
 Johnston, S., Hobbs, G., Vigeland, S., Kramer, M., Weisberg, J. M., & Lyne, A. G. 2006, *M.N.R.A.S.*, 364, 1397
 Karastergiou, A., von Hoensbroech, A., Kramer, M., Lorimer, D.R., Lyne, A.G., Doroshenko, O., Jessner, A., Jordan, C., & Wielebinski, R. 2001, *A&A*, 379, 270
 Komesaroff, M.M. 1970, *Nature*, 225, 612
 Krishnamohan, S., & Downs, G. S. 1983, *Ap.J.*, 265, 372.
 Kuz’mi, A. D. & Izvekova, V. A. 1996, in IAU Colloq. 160, Pulsars: Problems and Progress, ed. S. Johnston, M. A. Walker, & M. Bailes (ASP Conf. Ser. 105; San Francisco; ASP), 217.
 Malov, I. F., & Suleymanova, S.A. 1998, *Astron. Rep.* 42, 388 (MS98).
 Lorimer, D. R. *et al* 1998, *A&A Suppl.*, 128, 541
 Lyne, A.G., & Manchester, R.N. 1988, *M.N.R.A.S.*, 234, 477 (LM88)
 Lyubarskii, Y. E. & Petrova, S. 1998, *A&A*, 333, 181
 Manchester, R.N., Taylor, J.H., & Huguenin, G.R. 1975, *Ap.J.*, 196, 83.
 McKinnon, M. M., & Hankins, T. H. 1993, *A&A*, 269, 325 (MH93).
 Melrose. D, Miller. A, Karastergiou. A. & Luo, Q 2006, *M.N.R.A.S.*, 365, 638
 Mitra, D. 1999, Ph.D. Thesis, Jawaharlal Nehru University, New Delhi.
 Mitra, D., Konar, S., Bhattacharya, D., Hoensbroech, A. V., Seiradakis, J. H. & Wielebinski, R., 2000, *ASP Conf. Ser.* 202: IAU Colloq. 177: Pulsar Astronomy - 2000 and Beyond, 265
 Mitra, D. & Seiradakis, J. M. 2003, Proceeding of the 6th Hellenic Astronomical Conference, Penteli, Athens, Greece, 15-17 September 2003, P. G. Laskarides, ed., p. 205
 Mitra, D, & Rankin, J. M., 2002, *Ap.J.*, 577, 322 (MR02)

Mitra, D, Gupta, Y. & Kudale, S., 2005, "Polarization Calibration of the Phased Array Mode of the GMRT", URSI GA 2005, Commission J03a

Morris, D., Graham, D. A., Sieber, W., Jones, B. B., Seiradakis, J. H., & Thomasson, P. 1979, *A&A*, 73, 46

Ng, C. -Y. & Romani, R. W. 2004, *Ap.J.*, 601, 479

Petrova, S. A. 2006a, *M.N.R.A.S.*, 368, 1764

Petrova, S. A. 2006b, *M.N.R.A.S.*, 366, 1539

Radhakrishnan, V., & Cooke, D. J. 1969, *Ap. Lett.*, 3, 225

Radhakrishnan, V., & Rankin, J. M.. 1990, *Ap.J.*, 352, 258.

Ramachandran, R., Backer, D.C., Rankin, J.M., Weisberg, J.M., & Devine, K.E. 2004, *Ap.J.*, 606, 1167

Rankin J.M. 1983a, *Ap.J.*, 274 333

Rankin J.M. 1983b, *Ap.J.*, 274 359

Rankin J.M. 1986, *Ap.J.*, 301, 901

Rankin, J.M. 1990, *Ap.J.*, 352, 247 (R90)

Rankin J.M. 1993, *Ap.J.*, 405, 285 and *Ap.J. Suppl.*, 85, 145

Rankin J.M. 2006, *Ap.J.*, submitted

Rankin J.M., & Ramachandran, R. 2003, *Ap.J.*, 590, 411

Sirothia, S. 2000, M.Sc. thesis, University of Pune

Suleymanova, S.A., & Pugachev, V.D. 1998, *Astronomy Reports*, 42, 252

Suleymanova, S.A., & Pugachev, V.D. 2002, *Astronomy Reports*, 46, 34

Suleymanova, S.A. 2006, private communication

Swarup, G., Ananthakrishnan, S., Kapahi, V. K., Rao, A. P., Subrahmanyam, C. R., Kulkarni, & V. K. 1991, *Current Science* 60, 95.

Thomas, R.M.C., & Gangadhara, R. T. 2007, *A&A*, forthcoming

Weltevrede, P., Stappers, B. W., van den Horn, L. J., & Edwards, R. T. 2003, *A&A*, 412, 473

This paper has been typeset from a *T_EX/ L_AT_EX* file prepared by the author.